RESEARCH ARTICLE | AUGUST 15 1990

Description of tantalum deformation behavior by dislocation mechanics based constitutive relations

Frank J. Zerilli; Ronald W. Armstrong

Journal of Applied Physics 68, 1580–1591 (1990)
https://doi.org/10.1063/1.346636

Description of tantalum deformation behavior by dislocation mechanics based constitutive relations

Frank J. Zerilli and Ronald W. Armstrong[a)]
Research and Technology Department, Naval Surface Warfare Center, Silver Spring, Maryland 20903-5000

(Received 29 January 1990; accepted for publication 12 April 1990)

Dislocation mechanics based constitutive equation constants are determined for temperature, strain rate, work hardening, and polycrystal grain size influences on the deformation behavior of various tantalum materials. An analysis of the maximum load point strain provides a useful method of determining the work hardening constants. Different athermal stress constants and thermal activation related constants are obtained for certain groupings of the different tantalum materials. The variations are correlated with the annealing history of the materials and related to dislocation model parameters involved in the thermal activation strain rate analysis. Computed tantalum deformation results based on these constants are shown to agree with Gourdin's reported expanding ring test measurements and with the deformed shape of a Taylor cylinder impact test specimen.

I. INTRODUCTION

A. Why tantalum is interesting

Recent attention has been focused on developing constitutive equations for use in computational mechanics descriptions of complex metal deformations under dynamic loading[1] at strain rates up to and greater than $10^4\ s^{-1}$. Tantalum is a dense body centered cubic (bcc) metal of interest because it is relatively strong and ductile over a wide range of deformation rates and temperatures.[2,3] The yield strength of tantalum increases by more than 400% when tested[4,5] at temperatures from 298 to 77 K at a strain rate of the order of $10^{-4}\ s^{-1}$ or when tested[5] at strain rates from $10^{-4}\ s^{-1}$ to $4.9\times10^{3}\ s^{-1}$ at 298 K. Over these strain rate and temperature ranges, the uniform strain required to reach the maximum load point in a tensile test decreases from $\sim$0.25 to $\sim$0.05. The total range of deformation (and fracturing) behavior covers about 5% of the stress-temperature space reported for the fracture mechanism map of tantalum.[6]

B. Character of the constitutive relation

The character of any constitutive equation affects its utility for computational mechanics purposes. There is always the question of how reliably the equation may be extended past the strain, strain rate, and temperature conditions established by validating measurements. The model or physical basis for the equation is critical in this respect. The equation complexity can limit in a very meaningful way the efficient use of the equation in any lengthy computation. From this viewpoint, there is definite merit in obtaining a physically based constitutive equation that is not too complicated.

C. The bcc constitutive relation

A description has been given previously of two separate dislocation mechanics based constitutive relations for the deformation behavior of the fcc metal copper and the bcc metal iron.[1] The constitutive relations were applied to numerically modeling the impact of solid cylinders upon rigid targets[1,7] (Taylor tests). The bcc relation is written as follows:

$$\sigma = c_0 + B_0 e^{-\beta T} + K\epsilon^n, \tag{1}$$

where

$$\beta = \beta_0 - \beta_1 \ln \dot{\epsilon},$$

$$c_0 = \sigma_G + kl^{-1/2},$$

σ is the von Mises equivalent stress, ϵ is the equivalent strain, $\dot{\epsilon}$ is the strain rate, T is the absolute temperature, l is the average grain diameter, and σ_G is an athermal stress attributed to the initial dislocation density and the effect of solutes. The parameters $B_0, \beta_0, \beta_1, K, n$, and k as well as σ_G are considered to be constants to be obtained for a given material in a particular condition although several of the parameters have a relatively weak temperature and strain-rate dependence, in particular, σ_G and k. The upper and lower yield point phenomena typical of bcc metals are not described by Eq. (1), hence, at small strains, the equation applies only in an average sense.

II. DETERMINATION OF TEMPERATURE AND STRAIN-RATE COEFFICIENTS

A. Sources of experimental data

A number of sources of experimental data have been used to determine the parameters in Eq. (1) for tantalum. Relatively complete data were published by Hoge and Mukherjee[5] and the primary values of B_0, β_0, and β_1 were determined from their data. Their data were presented in graphs, so it was necessary to estimate numerical values for use in a fitting procedure. The estimation was done with a Tektronix 4957 digitizing tablet that converts graphical positions to numerical coordinates. The main sources of error in this process are the positional accuracy of the tablet and the (unknown) accuracy of the graphs. To obtain a rough estimate of the accuracy of the digitization, the claimed accuracy of

[a)] Permanent address: Department of Mechanical Engineering, University of Maryland, College Park, MD 20742.

the tablet of 0.025 in. may be compared with the dimensions of the figures. The deviations given in the results presented below are based upon this comparison and are believed to be conservative. Although Hoge and Mukherjee did not report experimental error estimates, the errors in such experiments are typically of the order of 10%, caused mostly by sample variation as opposed to measurement accuracy. Presuming the 10% figure, the experimental error is of the same order as the digitization error so that the deviations based upon the digitization error give a rough estimate of the overall error.

B. Athermal component of stress

The athermal component of stress, $c_0 + K\epsilon^n$, is determined from Hoge and Mukherjee's data on lower yield stress versus temperature (Ref. 5, Fig. 1) using the datum at 790 K, at which point the thermal component is assumed to be negligible. The lower yield stress at this point is 66 MPa with an estimated uncertainty of ∓ 20 MPa. For the purposes for which the model described by Eq. (1) is intended, it is satisfactory to assume that the constant value of the athermal component of stress to be used in Eq. (1) is the value at 298 K. To obtain this stress, it is assumed that the athermal stress has the same relatively weak temperature dependence as the shear modulus.[8] Featherston and Neighbours[9] report the shear modulus for tantalum at 300 K to be 81.8 GPa and at 140 K to be 85.2 GPa, varying linearly with temperature above 140 K. Assuming that the linear variation continues above 300 K, the shear modulus at 790 K is 71.4 GPa and therefore the athermal component of stress at 298 K is 76 MPa ∓ 20 MPa.

C. Determination of B_0 and β from temperature dependence of lower yield stress

Fixing $c_0 + K\epsilon^n$ at 76 MPa, a nonlinear least-squares fit (using the Levenberg–Marquardt method[10]) to Hoge and Mukherjee's lower yield stress versus temperature data at a strain rate of 10^{-4} s^{-1} gives

$$B_0 = 1110 \text{ MPa} \mp 80 \text{ MPa} \tag{2a}$$

and

$$\beta_{0.0001} = \beta_0 - \beta_1 \ln \dot{\epsilon} = (8.56 \mp 0.95) \times 10^{-3} \text{ K}^{-1}. \tag{2b}$$

A nonlinear least-squares fit in which $c_0 + K\epsilon^n$ is included in the parameters to be evaluated gives $c_0 + K\epsilon^n$ a value of (70 ∓ 45) MPa, the same B_0, and $\beta = (8.43 \mp 1.20) \times 10^{-3}$ K^{-1}.

D. Determination of β_0 and β_1 from strain-rate dependence of lower yield stress

From a nonlinear least-squares fit to Hoge and Mukherjee's data of lower yield stress versus strain rate at 298 K (Ref. 5, Fig. 6) it is determined that

$$\beta_1 T = 0.0975 \mp 0.0072 \tag{3a}$$

and

$$B_0 e^{-\beta_0 T} = 226 \mp 22 \text{ MPa} \tag{3b}$$

where, again, $c_0 + K\epsilon^n$ is fixed at 76 MPa (∓ 20). Thus

$$\beta_1 = (3.27 \mp 0.24) \times 10^{-4} \text{ K}^{-1} \tag{4a}$$

and

$$\beta_0 = (5.35 \mp 0.57) \times 10^{-3} \text{ K}^{-1}. \tag{4b}$$

The value of β_0 determined from Eqs. (2b) and (4a) is $(5.55 \mp 0.89) \times 10^{-3}$ K^{-1}.

III. DETERMINATION OF THE WORK HARDENING COEFFICIENTS

A. Difficulty in obtaining the work hardening coefficients

Determination of the work hardening coefficients K and n is not nearly as straightforward as determining the thermal activation coefficients. In principle, it is only necessary to do a nonlinear least-squares fit to the stress versus strain data. In practice, a wide range of results may be achieved depending upon the details of the fitting procedure. One problem in the fitting procedure is the presence of upper and lower yield points which make difficult any analysis of the small strain data. Unfortunately, these small strain data, particularly at low temperatures or high strain rates, are vital in definitively separating the strain-independent component of the yield stress from the strain-dependent part. There are then a wide range of combinations of coefficients K and n which will fit the experimental data reasonably well. Combined with the lack of precision in the data and the introduction of effects such as strain aging, it becomes almost impossible to choose work-hardening coefficients with any objectivity.

B. Obtaining the coefficients from the maximum load strain

A way around this difficulty clearly suggests itself when examining the load-elongation curves presented by Hoge and Mukherjee.[5] They show two sets of curves—one set in which the strain rate is fixed and the testing temperature is varied and another set in which the temperature is fixed and the strain rate is varied. In both sets a clearly defined maximum load point is observed whose position varies smoothly with temperature or strain rate. The value of the strain at maximum load increases with temperature and decreases with strain rate. This variation of strain at maximum load with temperature and strain rate is predicted for bcc metals by Eq. (1). This is exactly the reverse of the situation for fcc metals whose strain at maximum load decreases with temperature and increases with strain rate.[11]

C. Maximum load strain dependence on temperature and strain rate

At the maximum load point,

$$\sigma = d\sigma/d\epsilon, \tag{5}$$

where σ is the true flow stress and ϵ is the true strain. This condition is easily derived as follows: let F be the load on a tensile test specimen,

$$F = \sigma A = \sigma V/h, \tag{6}$$

where A is the cross-sectional area of the tensile test specimen, h is its length, and V is its volume. At constant strain

TABLE I. Maximum load strain as a function of temperature for tantalum at elongation rate $\dot{e} = 10^{-4}\,s^{-1}$ (from Hoge and Mukherjee[a]).

Temperature T (K)	Elongation e	True strain $\epsilon = \ln(1+e)$	Strain rate $\dot{\epsilon} = \dot{e}/(1+e)$ ($10^{-4}\,s^{-1}$)
78	0.054	0.052	0.949
115	0.094	0.090	0.914
144	0.119	0.112	0.894
202	0.158	0.147	0.864
298	0.275	0.243	0.784

[a] Reference 5, Fig. 7.

rate and temperature, and with V being presumed constant for plastic flow, the condition of maximum load is given by

$$\frac{dF}{dh} = \frac{V}{h}\left(\frac{d\sigma}{dh} - \frac{\sigma}{h}\right) = 0. \tag{7}$$

Equation (7) is equivalent to Eq. (5) because $d\epsilon = dh/h$. Applying the condition in Eq. (5) to the constitutive relation, Eq. (1), we obtain the expression

$$K(\epsilon^n - n\epsilon^{n-1}) + B_0 e^{-\beta T} + c_0 = 0. \tag{8}$$

Equation (8) determines the strain at maximum load as a function of temperature and strain rate for a bcc metal.

D. Obtain K and n by least-squares fit

Table I shows the maximum load point data as a function of temperature, derived from the stress-strain curves presented by Hoge and Mukherjee (Ref. 5, Fig. 7), and Table II shows the maximum load point data as a function of strain rate (Ref. 5, Fig. 8). Using the values of B_0, β_0, and β_1 determined from the lower yield stress data and assuming that the strain at the lower yield point is zero so that $c_0 = 76$ MPa, a nonlinear least squares fit of Eq. (8) to the maximum load strain versus temperature data in Table I yields values for K and n of 339 MPa and 0.489, respectively. A fit to the maximum load strain versus strain-rate data in Table II yields values for K and n of 331 MPa and 0.508, respectively. Taking the average of these results yields 335 MPa for K and 0.50 for n.

E. Correction for nonzero lower yield strain

Taking into account the observation that the plastic strain at the lower yield point has a nonzero value leads to modified values of B_0, c_0, K, and n. The modified values, denoted by primes, are determined by the equations:

$$B_0' = B_0(1 + e_{\mathrm{ly}}), \tag{9a}$$

$$c_0' = c_0(1 + e_{\mathrm{ly}}) - K'\epsilon_{\mathrm{ly}}^{n'}, \tag{9b}$$

where e_{ly} is the elongation and ϵ_{ly} is the true strain at the lower yield point. The modification of B_0 is not significant but the modifications to c_0, K, and n may be important.

F. Corrected values of K, n, and c_0

From an examination of the stress-strain curves in Hoge and Mukherjee's paper,[5] it was determined that a value of 0.014 represents an average value of the elongation at lower yield. A new value of c_0 may be calculated by substituting the previously determined values of c_0, K, and n into Eq. (9b). Using this new value of c_0, the nonlinear least-squares fitting procedure is repeated to determine improved values of K and n. This cycle is repeated until a set of values of c_0, K, and n is obtained which is consistent with both Eq. (9b) and the maximum load point data. In practice, only two or three iterations are required. The values of c_0, K, and n determined from the maximum load point versus temperature data are 27 MPa, 311 MPa, and 0.430, respectively. The corresponding values determined from the maximum load point versus strain rate data are 32 MPa, 304 MPa, and 0.449, respectively. The average values, rounded to two significant figures, are 30 MPa for c_0, 310 MPa for K, and 0.44 for n.

G. Comparison of computed and experimental maximum load strain

Figures 1(a) and 1(b) show the maximum load point (true) strain as a function of strain rate computed from Eq. (8), using the set of coefficients derived above. The computed curves are compared with Hoge and Mukherjee's data in Fig. 1(a) and with data reported by Regazzoni and Montheillet[2] in Fig. 1(b). Also plotted is the result computed using Eq. (8) with a somewhat smaller value of K of 250 MPa. This value of K gives an acceptable fit to the maximum load point data and gives a slightly better fit to the work hardening data of Regazzoni and Montheillet. There is substantial agreement between Regazzoni and Montheillet's data and those of Hoge and Mukherjee. Figures 2(a) and 2(b) show the computed maximum load strain as a function of temperature. Again, Hoge and Mukherjee's data are shown in Fig. 2(a) and, this time, data from a study by Bechtold[4] are shown in Fig. 2(b).

H. Estimating c_0 for other data

Because c_0 includes the effects of initial dislocation density, solutes, and grain size, it can be expected to vary from material to material. The values of c_0 for Bechtold's material and for that of Regazzoni and Montheillet which were used in Figs. 1(b) and 2(b) were estimated by comparing lower yield stresses corrected to the same strain, temperature, and strain rate.

To obtain c_0 for Bechtold's data we compare the lower yield stress at 298 K and $10^{-4}\,s^{-1}$ with the value of 154 MPa inferred from Hoge and Mukherjee's data (Ref. 5, Figs. 1, 7,

TABLE II. Maximum load strain as a function of strain rate for tantalum at 298 K (from Hoge and Mukherjee[a]).

Elongation rate $\dot{e}$ (s^{-1})	Elongation e	Strain rate $\dot{\epsilon} = \dot{e}/(1+e)$ (s^{-1})	True strain $\epsilon = \ln(1+e)$
0.0001	0.295	0.000077	0.259
0.08	0.175	0.068	0.162
170.	0.109	153.	0.103
4900.	0.060	4620.	0.059

[a] Reference 5, Fig. 8.

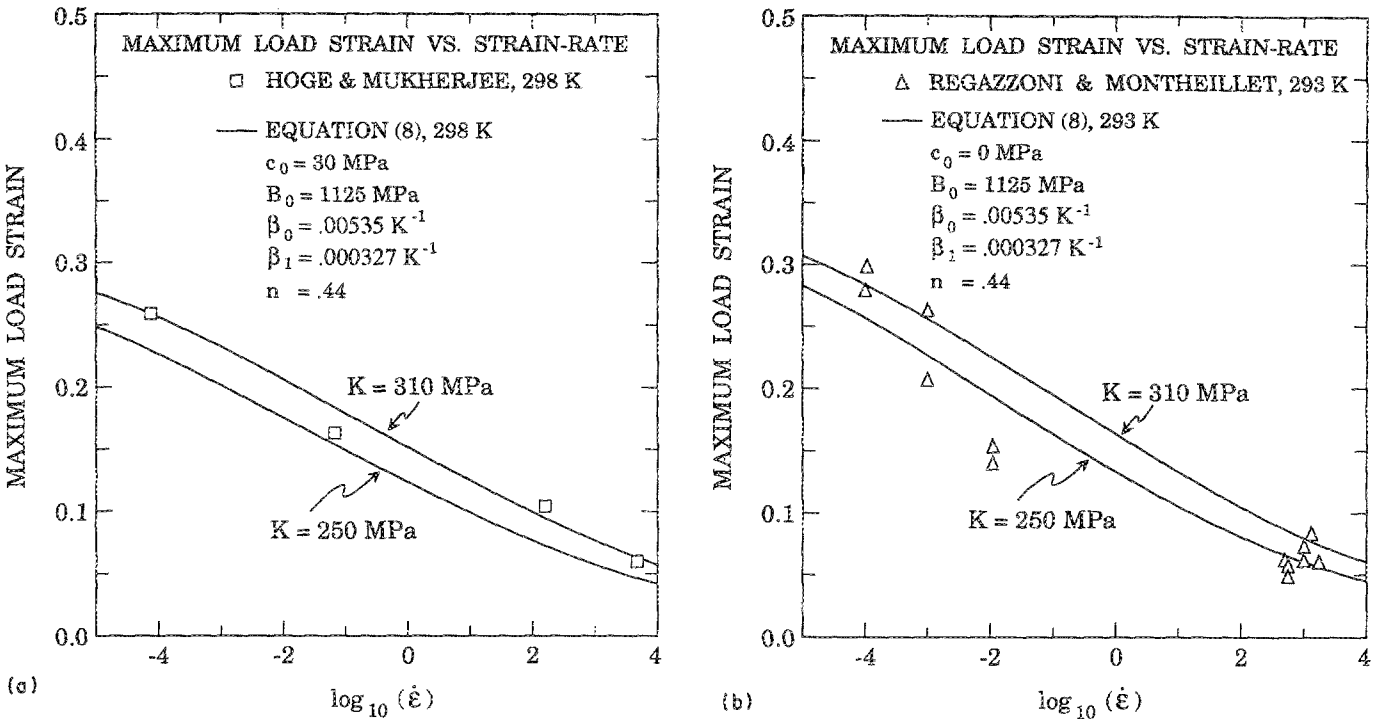

FIG. 1. Computed maximum load strain vs strain rate compared with experimental data. The curves are computed with Eq. (8) using the constants from Table III for comparison with the data of Hoge and Mukherjee (Ref. 5) in (a) and the data of Regazzoni and Montheillet (Ref. 2) in (b). The lower curves differ from the upper curves only in that K is set to 250 MPa. The temperature is 298 K in (a) and 293 K in (b).

and 8). Bechtold quotes a lower yield stress at 298 K and 2.8×10^{-4} s^{-1} of 274 MPa. From the parameters B_0, β_0, and β_1 already obtained, we find a 10 MPa correction for the strain rate difference. The plastic strain at lower yield for Bechtold's data at 298 K appears to be slightly larger than that for Hoge and Mukherjee's data. Assuming a value of 0.021 for ϵ_{iy} for Bechtold's data, we find a correction of approximately 10 MPa due to the extra strain hardening.

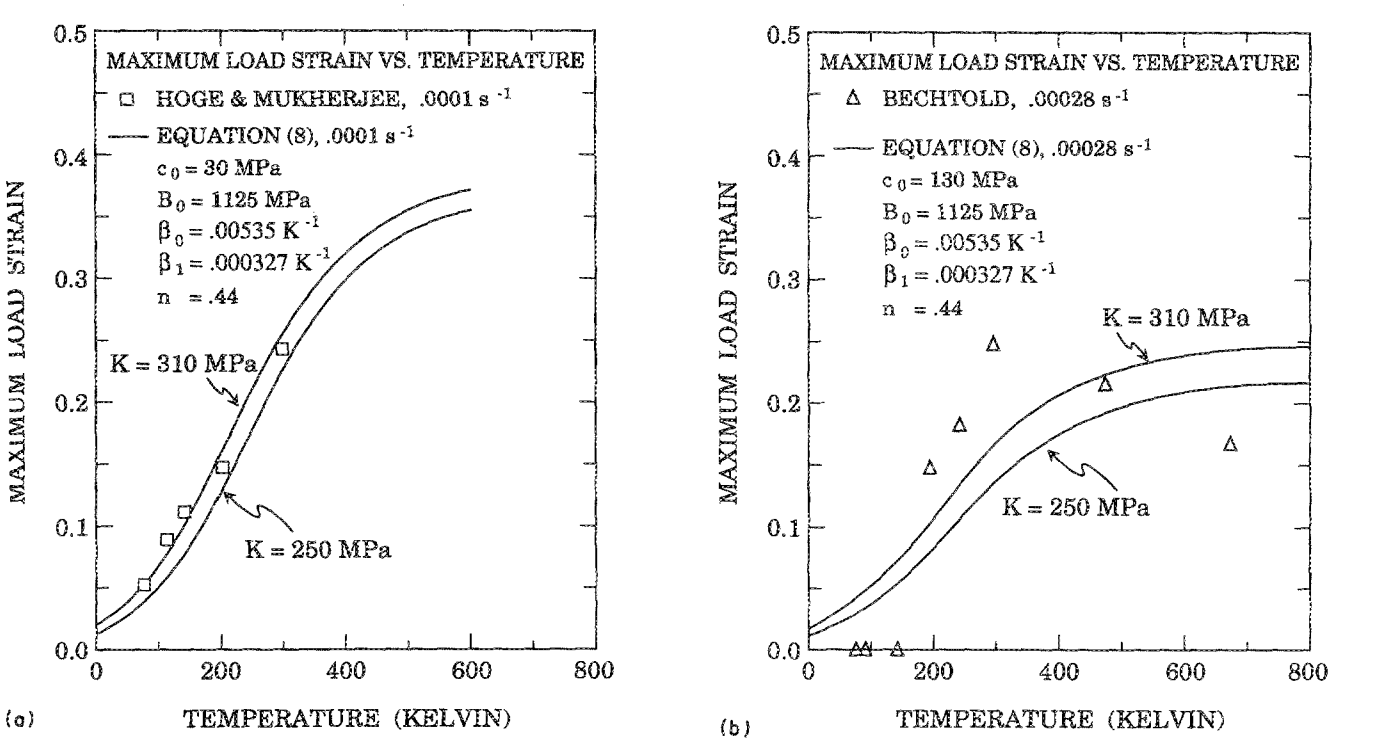

FIG. 2. Computed maximum load strain vs temperature compared with experimental data. The curves are computed with Eq. (8) using the constants from Table III for comparison with the data of Hoge and Mukherjee (Ref. 5) in (a) and the data of Bechtold (Ref. 4) in (b). The lower curves differ from the upper curves only in that K is set to 250 MPa. The strain rate is 10^{-4} s^{-1} in (a) and 2.8×10^{-4} s^{-1} in (b).

Thus c_0 for Bechtold's data is approximately 130 MPa. A similar comparison yields a c_0 of approximately 0 MPa for Regazzoni and Montheiliet's data.

I. Comparison of Bechtold's and Hoge and Mukherjee's results

Bechtold's data[4] are in very good agreement with those of Hoge and Mukherjee[5] in the temperature range between 200 and 300 K. At temperatures below 195 K, Bechtold concluded that no region of uniform strain occurred. Bechtold's two points at temperatures above 300 K show an unexpected reduction in the maximum load (uniform) strain. This reduction probably occurs because of the flow stress increase produced by the unusually large work hardening observed in the early stages of straining at these temperatures (473 and 673 K), a work hardening attributed by Bechtold to the effect of strain aging.

IV. STRAIN, TEMPERATURE, AND STRAIN-RATE DEPENDENCE OF THE FLOW STRESS

A. Comparison of computed stress-strain behavior with data of Hoge and Mukherjee

To see how well the predictions of Eq. (1), with the parameters determined above and summarized in Table III, compare with the experimental data reported by Hoge and Mukherjee,[5] true stress versus true strain curves are plotted for various temperatures at a strain rate of $10^{-4}\,s^{-1}$ in Fig. 3 and for various strain rates at 298 K in Fig. 4. The maximum load points determined for the experimental data may be compared with the maximum load locus predicted by Eq. (1). There is reasonably good agreement between the calculated and experimental curves.

The data in Fig. 3 cover a substantial fraction of the entire range of variation in the thermal component of stress for tantalum, for at 790 K the thermal component is virtually nonexistent while at 22 K the thermal component is close to the maximum possible value. As the temperature approaches zero the maximum load stress approaches approximately 1200 MPa and the maximum load strain approaches a value of 0.02 (this point is not shown in the figure but lies 100 MPa higher than the topmost point of the maximum load locus shown in Figs. 3 and 4). At high temperatures, the maximum load stress approaches 230 MPa and the maximum load strain approaches a theoretical maximum of 0.38. This high temperature limit is the right-most point on the maximum load locus shown in Figs. 3 and 4.

TABLE III. Summary of constitutive equation constants for tantalum obtained from data of Hoge and Mukherjee.[a]

$\sigma_G + kl^{-1/2} + K\epsilon_y^n$	76 MPa ∓ 20 MPa
$\sigma_G + kl^{-1/2}$	~30 MPa
B_0	1125 MPa ∓ 80 MPa
β_0	0.00535 K^{-1} ∓ 0.00057 K^{-1}
β_1	0.000327 K^{-1} ∓ 0.000024 K^{-1}
K	310 MPa
n	0.44

[a] Reference 5.

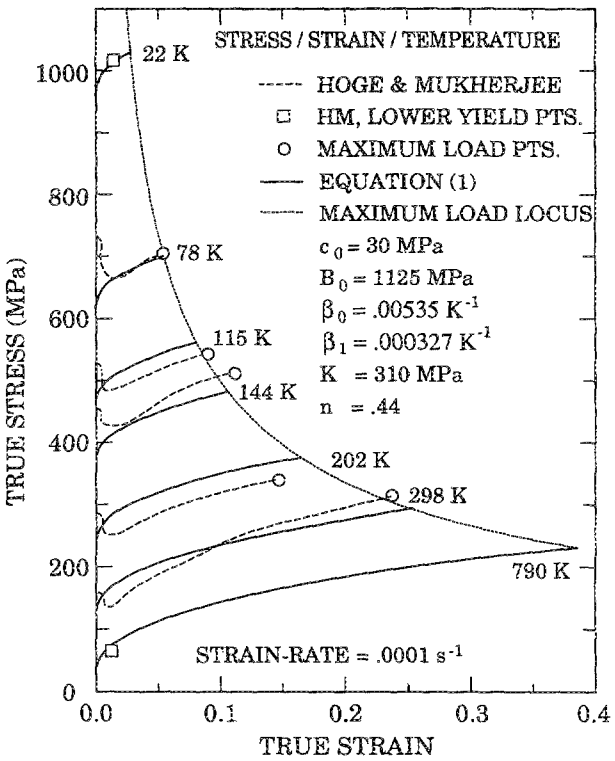

FIG. 3. Computed stress-strain curves compared with experimental data at temperatures of 22, 78, 115, 144, 202, 298, and 790 K for a strain rate of $10^{-4}\,s^{-1}$. The solid curves are computed with Eq. (1) using the constants in Table III. The dashed curves represent the data of Hoge and Mukherjee (Ref. 5). The dotted curve is the computed maximum load locus and the circles represent the experimental maximum load points.

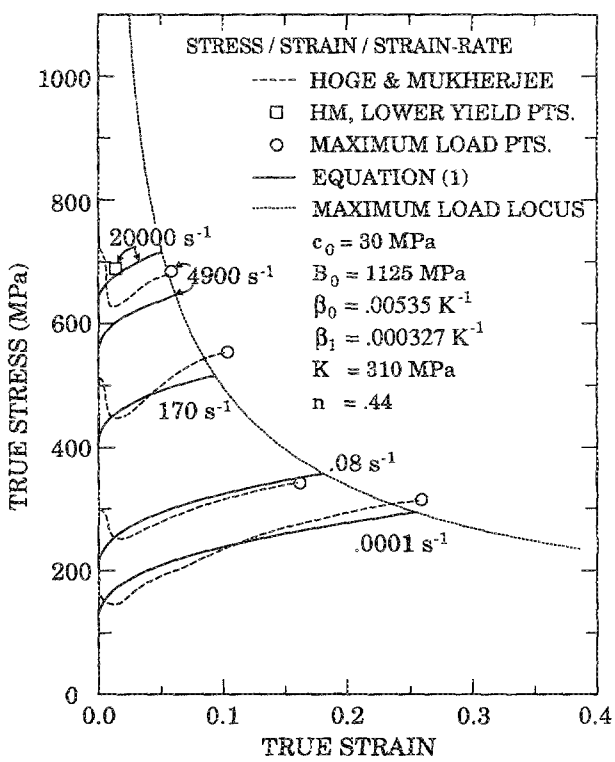

FIG. 4. Computed stress-strain curves compared with experimental data at strain rates of $10^{-4}\,s^{-1}$, 0.08 s^{-1}, 170 s^{-1}, 4900 s^{-1}, and 20 000 s^{-1} for a temperature of 298 K. The solid curves are computed with Eq. (1) using the constants in Table III. The dashed curves represent the data of Hoge and Mukherjee (Ref. 5). The dotted curve is the computed maximum load locus and the circles represent the experimental maximum load points.

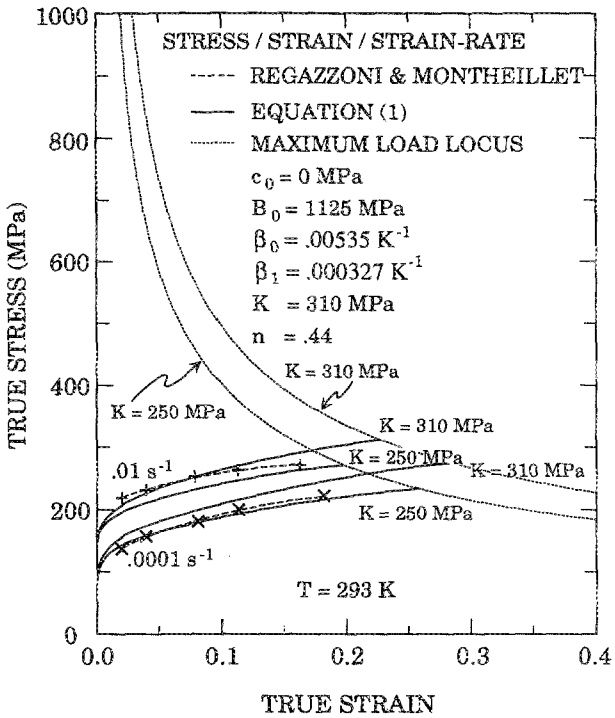

FIG. 5. Computed stress-strain curves compared with experimental data at strain rates of 10^{-4} s^{-1} and 10^{-2} s^{-1} for a temperature of 293 K. The solid curves are computed with Eq. (1) using the constants in Table III except for c_0 which is zero. The dashed curves represent the data of Regazzoni and Montheillet (Ref. 2). The dotted curves represent the computed maximum load locus. The lower set of computed curves differ from the upper set only in that K is set to 250 MPa.

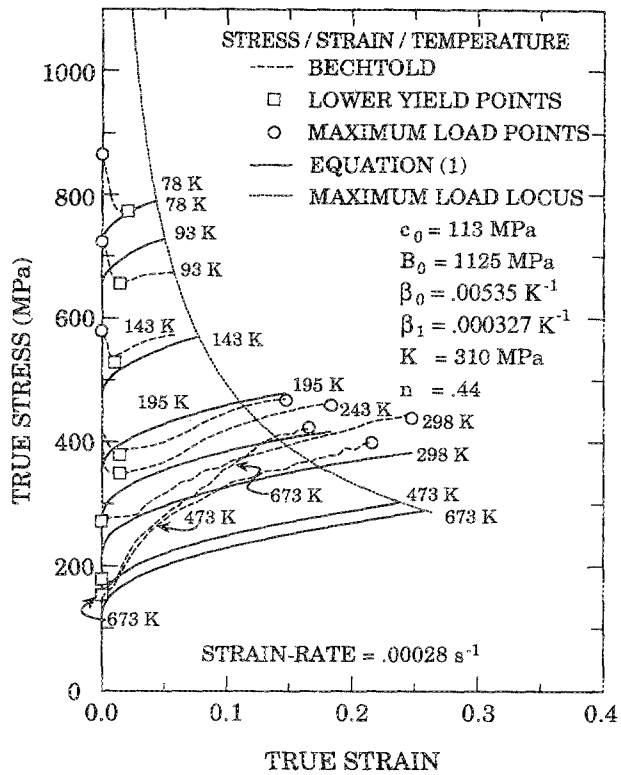

FIG. 6. Computed stress-strain curves compared with experimental data at temperatures of 78, 93, 143, 195, 243, 298, 473, and 673 K for a strain rate of 2.8×10^{-4} s^{-1}. The solid curves are computed with Eq. (1) using the constants from Table III except for c_0 which is set to 113 MPa. The dashed curves represent the data of Bechtold (Ref. 4). The dotted curve is the computed maximum load locus and the circles represent the experimental maximum load points.

B. Comparison of computed stress-strain behavior with data of other researchers

The comparison of stress-strain curves in Figs. 3 and 4 shows that Eq. (1) is capable of a reasonably accurate prediction of the flow stress and maximum load strain for data from which the parameters in the equation were obtained. There is still the question of how well this equation with these parameters can predict the flow properties of other tantalum material tested by other researchers. In this regard, a comparison with true stress-true strain data of Regazzoni and Montheillet is presented in Fig. 5 and of Bechtold in Fig. 6. In Fig. 5, the calculated values show reasonably good agreement with data at two different strain rates, although slightly better agreement is obtained by lowering the strain-hardening coefficient K from 310 to 250 MPa.

C. Large work hardening attributed to strain aging

In Fig. 6, wherein the data of Bechtold at several different temperatures are plotted, there is again reasonably good agreement. At the two highest temperatures, 473 and 673 K, the experimental data show that the flow stress has been raised substantially by the unusually large work hardening effect occurring in the early stage of straining. In fact, the initial work hardening at 673 K has raised the 673 K flow stress above the 473 K flow stress. However, the work hardening values at strains near the maximum load point are nearly as low as those for the computed curves at 473 and 673 K in Fig. 6. The result is a relatively reduced strain at the maximum load point in each case as is evident in both Figs. 6 and 2(b). The work hardening effect was attributed to strain aging by Bechtold. The strain aging behavior is consistent with the occurrence of a pronounced yield point behavior and a relatively high value of c_0. The absence of strain aging in the data of Regazzoni and Montheillet is clearly indicated by their smooth stress-strain curves. Table IV shows that the interstitial solute concentrations reported by Bechtold are consistent with an expected significant strain aging effect.

TABLE IV. Interstitial solute concentrations in the tantalum studied by several investigators.

Investigators		Carbon	Nitrogen	Oxygen
Hoge and Mukherjee[a]		?	?	?
Bechtold[b]		0.010	0.01	?
Regazzoni and Montheillet[c]		?	?	?
Mitchell and Spitzig[d]		0.0018	0.0006	0.0037
Mordike and Rudolph[e]		0.0005	0.0002	0.0018
Gilbert *et al.*[f]	Ta-C	0.0050	0.0012	0.0012
	Ta-N	0.0008	0.0022	0.0014
	Ta-O	0.0003	0.0012	0.0147

[a]Reference 5.
[b]Reference 4.
[c]Reference 2.
[d]Reference 13.
[e]Reference 14.
[f]Reference 12.

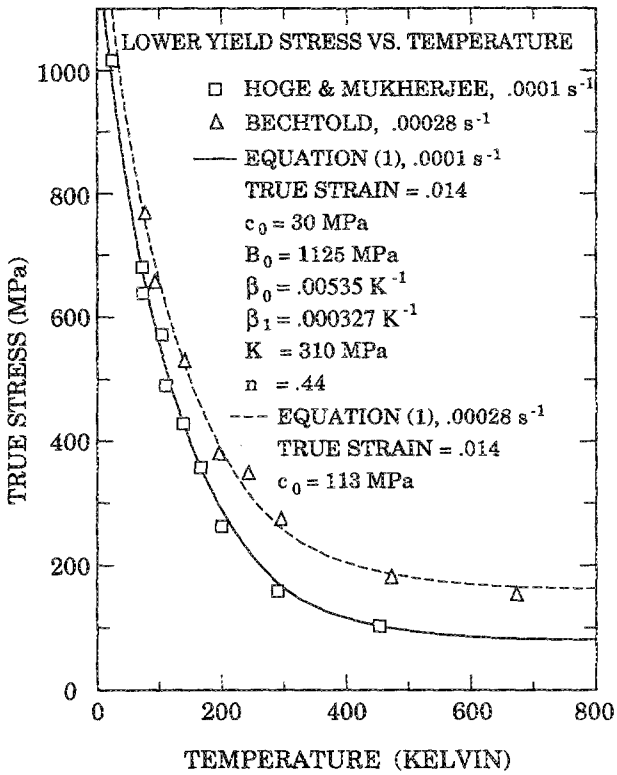

FIG. 7. Computed lower yield stress versus temperature compared with experimental data. The curves are computed with Eq. (1) using the constants from Table III except for c_0. The solid curve is computed with c_0 = 30 MPa and true strain of 0.014 at a strain rate of 10^{-4} s^{-1} to compare with the data of Hoge and Mukherjee (Ref. 5) represented by the squares. The dashed curve is computed with c_0 = 113 MPa and a true strain of 0.014 at a strain rate of 2.8×10^{-4} s^{-1} to compare with the data of Bechtold (Ref. 4) represented by the triangles.

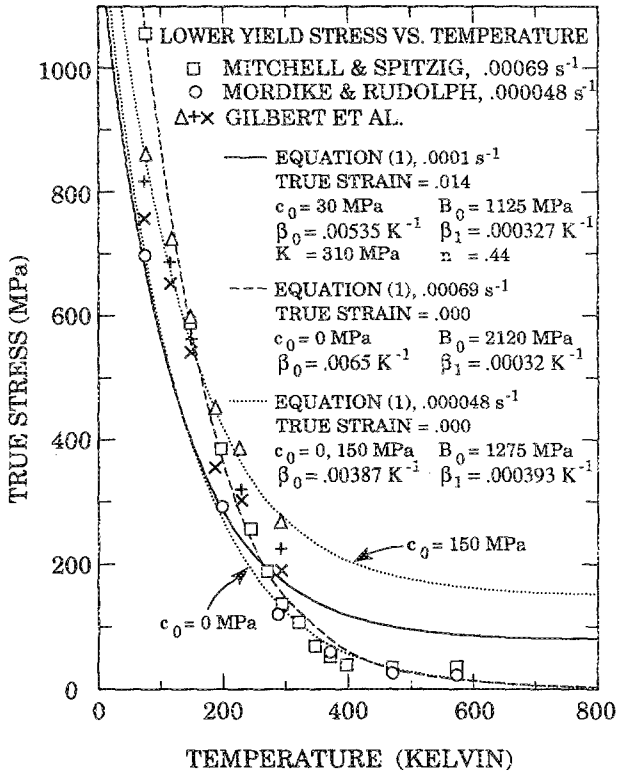

FIG. 8. Computed lower yield stress versus temperature compared with experimental data. The curves are computed with Eq. (1) using the constants from Table V. The solid curve is reproduced from Fig. 7. The dashed curve is computed for a strain rate of 6.9×10^{-4} s^{-1} to compare with the data of Mitchell and Spitzig (Ref. 13) represented by the squares. The two dotted curves are computed for a strain rate of 4.8×10^{-5} s^{-1} with c_0 = 0 MPa to compare with the data of Mordike and Rudolph (Ref. 14) represented by the circles and with c_0 = 150 MPa to compare with the data of Gilbert *et al.* (Ref. 12) represented by the triangles. The pluses and the ×'s represent the data of Gilbert *et al.* for differing solute concentrations.

D. Temperature dependence of the yield stress

The temperature variation of the lower yield stresses obtained by Hoge and Mukherjee[5] and Bechtold[4] is compared in Fig. 7 with the results computed with Eq. (1). It is seen that Eq. (1), with parameters (except for c_0) obtained from Hoge and Mukherjee's data (Table III), predicts results which agree very well with Bechtold's data if c_0 is changed to 113 MPa to allow for possible differences in solute and grain-size effects.

E. Variations in temperature and strain rate dependence of the yield stress

A further comparison of the results of Eq. (1), using the same parameters described above, with data obtained from a polycrystal study by Gilbert *et al.*,[12] and with single crystal data obtained by Mitchell and Spitzig[13] and Mordike and Rudolph[14] shows that these materials also exhibit different temperature and strain rate dependences. This is illustrated in Fig. 8 in which the lower yield stress variation with temperature is shown for the various studies and in Fig. 9, also, in which the lower yield stress variation with strain rate is shown.

F. Comparing single crystal and polycrystal results

In order to compare single crystal results with polycrystal results in the figures, the resolved shear stress of Mitchell

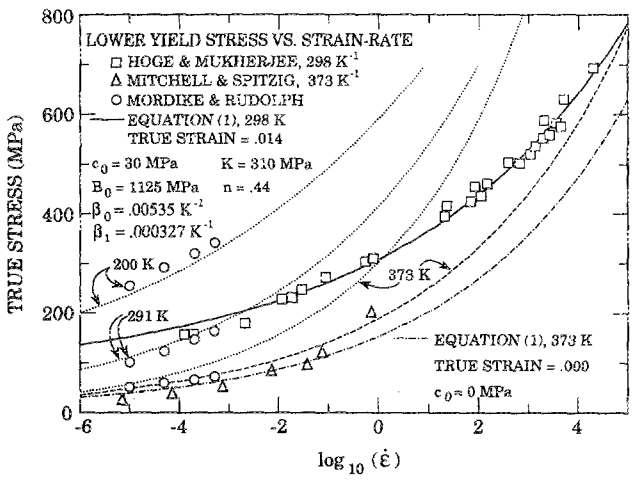

FIG. 9. Computed lower yield stress vs strain rate compared with experimental data. The curves are computed with Eq. (1) using the constants from Table V. The solid curve is computed for a temperature of 298 K at a strain of 0.014 to compare with the data of Hoge and Mukherjee (Ref. 5) represented by squares. The dotted curves are computed at temperatures of 200, 291, and 373 K for zero strain to compare with the data of Mordike and Rudolph (Ref. 14) represented by the circles. The dashed curve is computed at 373 K and zero strain to compare with the data of Mitchell and Spitzig (Ref. 13) represented by the triangles. The dot-dashed curve is computed for a temperature of 373 K and zero strain, but using the constants fitting the Hoge and Mukherjee data (Ref. 5).

and Spitzig[13] and of Mordike and Rudolph[14] have been multiplied by a Taylor orientation factor of 2.9 to give an equivalent polycrystal flow stress. The shear strain rates of Mordike and Rudolph were divided by 2.9 to obtain equivalent polycrystal strain rates. Mitchell and Spitzig apparently quote elongation rates so these were multiplied by the factor 2.14 calculated for their quoted orientation to obtain glide plane shear strain rates and then divided by 2.9 to obtain equivalent polycrystal strain rates. This procedure gives what might seem to be excessively large values for the Mitchell and Spitzig yield stresses, but, nevertheless, it seems the best way to compare the single crystal with polycrystal data. It should be noted that the relatively high slip stress levels were observed by Mitchell and Spitzig to lead to deformation twinning of the crystals at 4.2 K. A twinning shear stress of 419 MPa, equivalent to a polycrystal friction stress of 1215 MPa, was measured at 4.2 K.

G. Comparison of computed temperature and strain rate dependence with experimental data

The yield stress versus temperature data of some authors are plotted in Fig. 8 together with the prediction, reproduced from Fig. 7, of Eq. (1) for the Hoge and Mukherjee data (solid line). It can be seen that lowering c_0 to zero to account for the lesser solute effects and lack of grain-boundary effect would not fit the low temperature data well. The lower dotted curve was computed with Eq. (1) with parameters adjusted to fit the Mordike and Rudolph data.[14] These parameters also give a good fit to the Gilbert *et al.*[12] data as is shown by the upper dotted curve which is simply the lower curve displaced upward by 150 MPa to account for increased solute and grain-size effects. The dashed curve represents the results of Eq. (1) with parameters adjusted to fit the Mitchell and Spitzig data.[13] The results in this case clearly show a behavior which is expected on the basis of the thermal activation model from which Eq. (1) is derived, that is, β_1 is essentially unchanged, while B_0 and β_0 have increased to follow the low temperature behavior of the yield stress (see Sec. V). It is also possible to obtain reasonable predictions with Eq. (1) for the Mordike and Rudolph data by retaining the Hoge and Mukherjee β_0 and β_1 but increasing B_0 to 1360 MPa. The best fit thermal term parameters for the various studies are listed in Table V.

TABLE V. Comparison of constitutive equation constants fitting the results of several investigators.

Investigators	c_0 (MPa)	B_0 (MPa)	β_0 (K^{-1})	β_1 (K^{-1})
Hoge and Mukherjee[a]	30	1125	0.00535	0.000327
Bechtold[b]	130	...	...	...
Mordike and Rudolph[c]	0	1275	0.00387	0.000393
Gilbert, *et al.*[d]	150	...	...	...
Mitchell and Spitzig[e]	0	2120	0.0065	0.00032

[a]Reference 5.
[b]Reference 4.
[c]Reference 14.
[d]Reference 12.
[e]Reference 13.

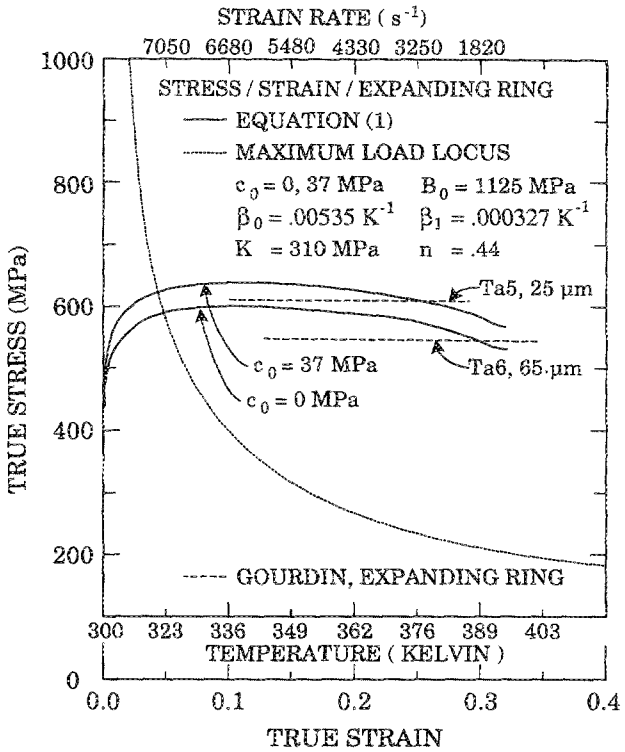

FIG. 10. Computed stress-strain curves compared with expanding ring experimental data of Gourdin (Ref. 15). The solid curves are computed with Eq. (1) using the constants from Table III except that $c_0 = 0$ MPa for the lower curve and $c_0 = 37$ MPa for the upper curve. The temperature and strain rate vary with strain as indicated. The dotted curve is the computed maximum load locus. The dashed lines represent Gourdin's data for two grain sizes, 25 and 65 μm.

H. Comparison of computed values with high strain rate expanding ring data

An interesting comparison of results at high strain rates is made with data reported by Gourdin[15] for electromagnetically driven expanding rings of tantalum having two different grain sizes, 25 and 65 μm. The predictions of Eq. (1) using the parameters derived from the Hoge and Mukherjee data are shown in the stress-strain curves in Fig. 10. For each strain, the values of temperature and strain rate obtained by integrating Gourdin's reported temperature and strain rate as functions of time are used. Two curves (solid lines) separated by 37 MPa are shown, corresponding to the two experimental curves (dashed lines) for two different grain sizes, 65 and 25 μm. The value of 37 MPa for the grain size difference was obtained using a value of k of 15 MPa $mm^{1/2}$ in the grain size term in Eq. (1). The experimental separation of the curves is greater, but this is consistent with the expectation that k increases somewhat with decrease in temperature or increase in strain rate as observed by Gilbert *et al.*[12] The determination of the value of k is discussed later in Sec. VI. There is reasonably good agreement between the calculated curves and the experimental data. A maximum load locus is plotted (dotted line) in the figure to show that the range of the experimental data lies entirely in the region of predicted tensile instability. Therefore, there must have been a significant tendency for the ring to "bead" although

this may have been ameliorated by the effect of strain rate hardening.

V. DISLOCATION MODEL INTERPRETATION OF THERMAL ACTIVATION PARAMETERS

A. Low temperature/large stress thermal activation approximation

In an approximation[1] of the thermal activation model for temperatures near zero,

$$B_0 = mG_0/A_0 b, \tag{10}$$

$$\beta_0 = \frac{1}{T}\ln\left(\frac{A}{A_0}\right) + \frac{k}{G_0}\ln\left(\frac{m'bNv_0}{\dot{m}}\right), \tag{11}$$

$$\beta_1 = k/G_0, \tag{12}$$

where G_0 is the Gibbs free energy of activation for zero applied stress, A is the activation area, b is the Burger's vector, N is the areal density of dislocations, v_0 is the limiting dislocation velocity, m and m' are orientation factors, T is the absolute temperature, k is Boltzmann's constant, and A_0 is the area of activation at absolute zero temperature. This approximation is valid for the large values of stress occurring at low temperatures. At these large stresses the activation area is approximately constant with the value A_0.

B. General thermal activation model

Over a broader range of smaller stress values the activation area becomes inversely proportional to the effective thermal stress component[16,17]. In general, therefore, the area of activation may be written in the form

$$A = A_0 + W_0/b\tau_{\mathrm{Th}}, \tag{13}$$

where W_0 has the units of energy. Alternatively, the area of activation may be written in the form

$$A = \begin{cases} W_0/b\tau_{\mathrm{Th}}, & \tau_{\mathrm{Th}} \leqslant W_0/A_0 b, \\ A_0, & \tau_{\mathrm{Th}} > W_0/A_0 b. \end{cases} \tag{14}$$

Substituting this expression in the equation describing the thermally activated motion of dislocations,

$$\dot{\gamma} = m'Nbv_0 e^{-G/kT}, \tag{15a}$$

where

$$G = G_0 - \int_{\tau_{\mathrm{Th}}}^{0} V\,d\tau \tag{15b}$$

and

$$V = Ab, \tag{15c}$$

the equation,

$$\sigma_{\mathrm{Th}} = \begin{cases} B_0 e^{-\beta T}, & \sigma_{\mathrm{Th}} \leqslant \sigma_c, \\ \sigma_c[1 + \ln(B_0/\sigma_c) - \beta T], & \sigma_{\mathrm{Th}} > \sigma_c, \end{cases} \tag{16}$$

determining the flow stress, is obtained. The constants in Eqs. (15) and (16) are related to the basic thermal activation parameters by

$$\sigma_c = W_0 m/A_0 b, \tag{17a}$$

$$B_0 = \sigma_c \exp(G_0/W_0), \tag{17b}$$

$$\beta = \beta_0 - \beta_1 \ln \dot{\epsilon}, \tag{17c}$$

$$\beta_0 = (k/W_0)\ln \dot{\epsilon}_0, \tag{17d}$$

and

$$\beta_1 = k/W_0, \tag{17e}$$

where $\sigma_{\mathrm{Th}} = m\tau_{\mathrm{Th}}$, $\dot{\epsilon} = \dot{\gamma}/m$, and m is the orientation factor.

C. Upper limit to A_0 for tantalum

In the data examined in this paper, there is no detectable deviation from the $e^{-\beta T}$ dependence, indicating that $\sigma_c > 1000$ MPa. From the value of W_0 determined from β_1, an upper limit of 10^{-22} cm^3 is calculated for $A_0 b$.

D. Effects of annealing and interstitial solutes

Because β_1 depends only on the energy W_0 characterizing the thermal activation process, it should be insensitive to differences in annealing or solute concentrations (excluding strain aging and yield point phenomena). B_0 and β_0, however, depend on thermal activation parameters which ought to be more sensitive to dislocation structure. β_0 depends also on the dislocation density and B_0 depends on A_0 as well as on G_0 and W_0. Therefore, both of these parameters might be expected to vary with annealing differences.

E. Variations in the thermal activation parameters

The two thermal activation parameters, W_0 and $\dot{\epsilon}_0$ can be determined from β_0 and β_1 via Eqs. (17d) and (17e). These two parameters are compared for the various studies in Table VI. There is a relatively small variation in W_0. It is the annealing differences and, to a lesser extent, the interstitial solute differences, apparently, which separate the experimental data into two main classes: Mordike and Rudolph,[14] Mitchell and Spitzig,[13] and Gilbert *et al.*[12] have the most thoroughly annealed material as opposed to the lesser annealed material of Hoge and Mukherjee,[5] Bechtold,[4] and Regazzoni and Montheillet.[2] This is reflected in the significant differences in $\dot{\epsilon}_0$ shown in Table VI. The dislocation density is probably the main factor influencing this quantity. For the usual commercially available stock material, the parameters derived from the Hoge and Mukherjee data would seem to be appropriate. Unusually well-annealed material would require larger values of the threshold stress B_0 and possibly altered values of β_0.

TABLE VI. Comparison of thermal activation parameters from the results of several investigators.

Investigators	W_0 (10^{-20} J)	$\dot{\epsilon}_0$ (s^{-1})
Hoge and Mukherjee[a]	4.2	1.3×10^{7}
Bechtold[b]	...	...
Mordike and Rudolph[c]	3.5	1.9×10^{6}
Gilbert *et al.*[d]	...	...
Mitchell and Spitzig[e]	4.3	6.6×10^{8}

[a]Reference 5.
[b]Reference 4.
[c]Reference 14.
[d]Reference 12.
[e]Reference 13.

F. Comparisons of yield stress versus strain rate studies

Only Hoge and Mukherjee,[5] Mordike and Rudolph,[14] and Mitchell and Spitzig[13] have reported data on the yield stress variation with strain rate for a reasonably wide range of strain rates. These data are shown in Fig. 9 and compared with the predictions of Eq. (1). The solid curve shows the (not unexpected) good fit of Eq. (1) to the Hoge and Mukherjee data. The dot-dashed curve shows the prediction of Eq. (1) with the same parameters but for 373 K and displaced downward to $c_0 = 0$ and zero true strain to compare with the Mitchell and Spitzig data. The dashed curve shows the prediction of Eq. (1) using the parameters specifically determined to fit the Mitchell and Spitzig data as previously discussed. The dotted curves show the prediction of Eq. (1) using the parameters specifically determined to fit the Mordike and Rudolph data at the three temperatures 200, 291, and 373 K.

G. How annealing may affect the temperature and strain-rate dependences

The area of activation A can be obtained from the slope of the curves in Fig. 9 from the relation

$$A = mkT \Big/ b\left(\frac{\partial \sigma}{\partial \ln \dot{\epsilon}}\right)_T . \tag{18}$$

Thus, the steeper slopes for the results of Mordike and Rudolph[14] at 291 K compared with Hoge and Mukherjee[5] at 298 K imply smaller activation areas in the former case. The Mordike and Rudolph results are in reasonable agreement with those of Mitchell and Spitzig[13] at 373 K. The relative values of the activation area inferred from Fig. 9 are consistent with the temperature dependences shown for these same three investigations in Fig. 8. From the relation

$$A = mk \ln\left(\frac{\dot{\epsilon}}{\dot{\epsilon}_0}\right) \Big/ b\left(\frac{\partial \sigma}{\partial T}\right)_{\dot{\epsilon}} . \tag{19}$$

it can be seen that the smaller temperature dependence shown for the Hoge and Mukherjee results indicates a relatively larger activation area.

The differences in activation areas are possibly explained theoretically by differences in the individual dislocation line properties that can be reasoned to apply for each investigation. The relatively pure, well-annealed single crystals of Mordike and Rudolph initially should have contained dislocations in low energy Peierls valleys, with relatively few kinks of any size on the dislocation lines. Hence, small values of activation area should have occurred for dislocation movement by this mechanism. Leslie and Sober[18] have reported results on the increased temperature dependence of well-annealed pure iron compared with iron prestrained during specimen preparation. An initial deformation induced dislocation structure would produce dislocations in a greater energy state with larger kinks corresponding to a larger activation area, a lower thermal stress, and lesser strain rate dependence of the flow stress. This behavior is characteristic of dislocations in bcc lattices but not fcc lattices where dislocation intersections control the thermal activation stress.

VI. EFFECT OF GRAIN BOUNDARIES

A. The Hall–Petch grain size dependence

The constitutive relation, Eq. (1), contains a term proportional to the inverse square root of the average grain diameter. In order to determine a value for the constant of proportionality, k, lower yield stress values were plotted versus the reciprocal square root of polycrystal grain diameter for various tantalum studies[2,4,5,12–15] These values are shown in Fig. 11, and compared with the Hall–Petch relation[19]

$$\sigma_y = \sigma_0 + k l^{-1/2}, \tag{20}$$

where l is the average grain diameter, k is the microstructural stress intensity, and σ_0 is the friction stress for plastic flow within the polycrystal grains. As noted, the majority of results were obtained at approximately 300 K and at a strain rate of approximately $10^{-4}\ s^{-1}$.

B. Hall–Petch measurements

Gilbert *et al.*[12] have reported lower yield point stresses for one polycrystal grain size corresponding to $l^{-1/2} = 2.83\ mm^{-1/2}$ and have given σ_0 and k values for three well-annealed tantalum materials containing various oxygen, nitrogen, or carbon solutes (see Table IV). The yield stress data are shown at this grain size in Fig. 11, with Hall–Petch lines drawn at the reported slope values for each main interstitial alloy. The σ_0 values obtained for the intersection of these lines with the ordinate at $l^{-1/2} = 0$ occur near to the range of values reported by Gilbert *et al.*[12] The higher strength results that are shown in Fig. 11 for Gilbert *et al.* are attributed to relatively large values of σ_0. Nevertheless, low k values are indicated for their relatively pure, well-annealed material, particularly of low nitrogen and oxygen content, although containing carbon.

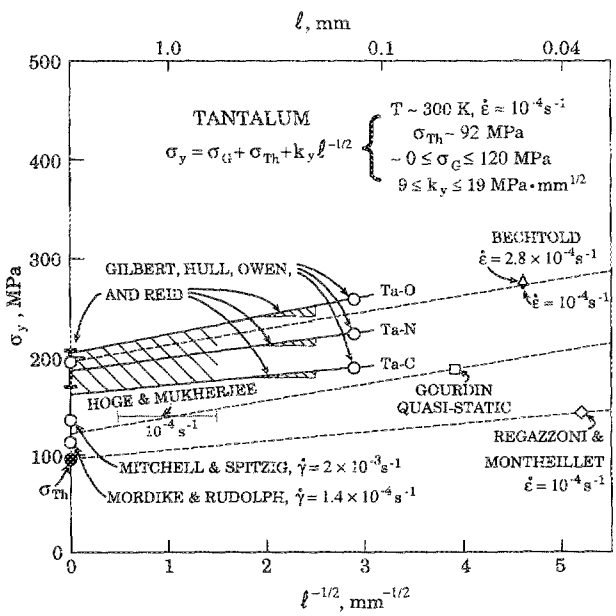

FIG. 11. Yield stress versus inverse square root of grain size.

C. Single crystal measurements

Also at $l^{-1/2} = 0$ in Fig. 11, computed values of $\sigma_0 = m\tau_0$ are shown with $m = 2.9$ and average critical resolved shear stress, τ_0, of approximately 40 and 48 MPa, taken from Mordike and Rudolph[14] and Mitchell and Spitzig,[13] respectively. A value of σ_{Th} of 92 MPa is shown at $l^{-1/2} = 0$, as computed from Eq. (1) with the B_0, β_0, and β_1 values given in Table III. The computed σ_{Th} is less than the σ_0 values obtained from the single crystal data because the single crystal data also contain an athermal component of stress.

D. Regazzoni and Montheillet results

Regazzoni and Montheillet[2] reported their sintered polycrystal material to contain a range of grain diameters between 20 and 100 μm giving an average value of $l^{-1/2}$ of 5.2 mm$^{-1/2}$, as shown in Fig. 11. This material and the recrystallized material reported by Hoge and Mukherjee,[5] placed at an estimated average grain diameter of 1.0 mm in Fig. 9, are shown to have polycrystal yield strengths just greater than the ordinate σ_0 value determined from single crystal measurements. The Regazzoni and Montheillet results are shown to extrapolate to $l^{-1/2} = 0$ at a lowest possible value of $\sigma_G = 0$ employing a smallest value of $k = 9$ MPa mm$^{1/2}$, as reported by Gilbert *et al.*[12] for their 50 ppm carbon containing material. No evidence of strain aging is present in the relatively smooth stress-strain curves of Regazzoni and Montheillet (see Fig. 5). On the other hand, Bechtold[4] reported a pronounced influence of strain aging on his results (see Fig. 6), exhibiting in Fig. 11 the highest σ_0 and k values.

E. Values of the Hall–Petch microstructural stress intensity

All of the experimental measurements in Fig. 11 are shown to be at or above the computed thermal stress value $\sigma_{Th} \sim 92$ MPa at 300 K and strain rate of about 10^{-4} s^{-1}. The combination of σ_G and $kl^{1/2}$ stress components indicated in the figure are in agreement with c_0 values ranging from essentially zero, for Regazzoni and Montheillet, to 130 MPa, for Bechtold, allowing in both cases for a work hardening contribution to the yield stress values described in earlier figures. The total results may be interpreted in terms of solutes and grain size with the Hall–Petch microstructural stress intensity k in the range between 9 and 19 MPa mm$^{1/2}$.

VII. CONCLUSION

The dislocation mechanics based Eq. (1) predicts the overall stress-strain behavior of a number of tantalum materials reasonably well, including their tensile instability behavior, even though yield point phenomenon, strain aging, and texture effects are neglected. Variations in some of the parameters in the constitutive relation are correlated with interstitial solute content, annealing differences, and grain size and are shown to be reasonable in terms of a dislocation model.

Satisfactory agreement has been obtained between computed stress-strain curves and expanding ring test results.

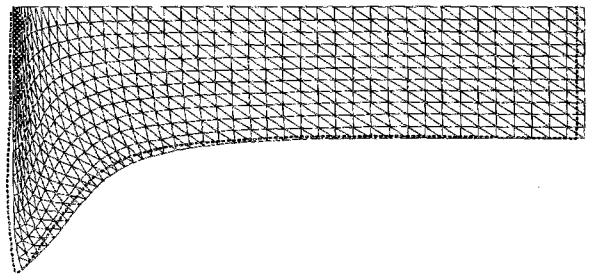

FIG. 12. Taylor cylinder test computation (McKirgan and Barker, Ref. (20) compared with experiment (Holt and Mock, Ref. 21). Solid lines show the result computed with Johnson's EPIC-2 material dynamics code (Ref. 7) and Eq. (1) with the constants from Table III. The dotted line shows the outline of the experimental result for an impact velocity of 186 ms^{-1}.

Additional evidence for the usefulness of the equation for the numerical modeling of tantalum deformation is provided in Fig. 12. It shows a computation[20] of a Taylor cylinder impact test[21] in which a reasonably pure, polycrystalline tantalum cylinder was propelled against a hardened steel target at 186 ms^{-1}. The resulting deformation is shown to compare very closely with that computed with Eq. (1) using the constants in Table III.

ACKNOWLEDGMENTS

The authors wish to thank William Gourdin of Lawrence Livermore National Laboratory for providing temperature and strain-rate data for his expanding ring experiment, and John McKirgan and Donald Barker of the University of Maryland, and William Holt and Willis Mock of NSWC for providing their unpublished cylinder impact computation and experimental data, respectively. This work was supported by the Office of Naval Technology. The authors also wish to thank K. W. Reed and P. A. Walter of NSWC for their encouragement and support for this work.

[1] F. J. Zerilli and R. W. Armstrong, J. Appl. Phys. **61**, 1816 (1986).
[2] G. Regazzoni and F. Montheillet, in *Mechanical Properties at High Rates of Strain*, edited by J. Harding, Conf. Series No. 70 (Institute of Physics, London, 1984), p. 63.
[3] D. J. Steinberg and C. M. Lund, J. Phys., Coll. C3, Suppl. 9, **49**, 433 (1988); J. Appl. Phys. **65**, 1528 (1989).
[4] J. H. Bechtold, Acta Metall. 3, 249 (1955).
[5] K. G. Hoge and A. K. Mukherjee, J. Mater. Sci. **12**, 1666 (1977).
[6] C. Gandhi and M. F. Ashby, Acta Metall. **27**, 1565 (1979).
[7] G. R. Johnson and W. H. Cook, in Proceedings of the Seventh International Symposium on Ballistics, The Hague, The Netherlands, 1983, p. 541.
[8] A. Seeger, *Kristallplastizitat, Handbuch der Physik VII/2, Crystal Physics II*, edited by S. Flugge (Springer, Berlin, 1958), pp. 1–264.
[9] F. H. Featherston and J. R. Neighbours, Phys. Rev. **130**, 1324 (1963).
[10] W. H. Press, B. P. Flannery, S. A. Teukolsky, and W. T. Vetterling, *Numerical Recipies* (Cambridge Univiversity Press, Cambridge, 1986), p. 523.
[11] F. J. Zerilli and R. W. Armstrong, in *Shock Waves in Condensed Matter 1989*, edited by S. C. Schmidt, N. C. Holmes, and J. N. Johnson (Elsevier, London, 1990), to be published.
[12] A. Gilbert, D. Hull, W. S. Owen, and C. N. Reid, J. Less-Common Metals **4**, 399 (1962).
[13] T. E. Mitchell and W. A. Spitzig, Acta Metall. **13**, 1169 (1965).
[14] B. L. Mordike and G. Rudolph, J. Mater. Sci. **2**, 332 (1967).
[15] W. H. Gourdin, in Proceedings of the Fourth International Conference on

the Mechanical Properties of Materials at High Rates of Strain, Oxford, England, 20–22 March 1989, edited by John Harding, to be published.
[16]R. W. Armstrong and J. D. Campbell, in *The Microstructure and Design of Alloys, Proceedings of the Third International Conference on the Strength of Metals and Alloys*, Vol. 1 (Institute of Metals and the Iron and Steel Institute, Cambridge, UK, 1973), p. 529.
[17]B. L. Mordike, Z. Metallkde. **53**, 586 (1962).
[18]W. C. Leslie and R. J. Sober, Trans. ASM **60**, 99 (1967).
[19]R. W. Armstrong, in *The Yield, Flow and Fracture of Polycrystals*, edited by T. N. Baker (Applied Science, London, 1983), p. 1.
[20]J. B. McKirgan and D. B. Barker, University of Maryland, unpublished computation.
[21]W. H. Holt and W. Mock, Jr., Naval Surface Warfare Center, unpublished test result.